A-site-driven ferroelectricity in strained ferromagnetic La_2NiMnO_6 thin films

R. Takahashi,[1,*] I. Ohkubo,[2,3] K. Yamauchi,[4] M. Kitamura,[2] Y. Sakurai,[2] M. Oshima,[2,5] T. Oguchi,[4,6] Y. Cho,[7] and M. Lippmaa[1]

[1]*Institute for Solid State Physics, University of Tokyo, 5-1-5, Kashiwanoha, Kashiwa, Chiba 277-8581, Japan*

[2]*Department of Applied Chemistry, School of Engineering, University of Tokyo, 7-3-1 Hongo, Tokyo 113-8656, Japan*

[3]*National Institute for Materials Science, Tsukuba 305-0044, Japan*

[4]*Institute of Scientific and Industrial Research, Osaka University, Ibaraki, Osaka 567-0047, Japan*

[5]*Synchrotron Radiation Research Organization, University of Tokyo, Tokyo 113-8656, Japan*

[6]*JST-CREST, Kawaguchi, Saitama, 332-0012, Japan*

[7]*Research Institute of Electrical Communication, Tohoku University, Sendai, 980-8577, Japan*

(Received 17 December 2014; revised manuscript received 29 January 2015; published 20 April 2015)

We report on theoretical and experimental investigation of *A*-site-driven ferroelectricity in ferromagnetic La_2NiMnO_6 thin films grown on $SrTiO_3$ substrates. Structural analysis and density-functional theory calculations show that epitaxial strain stretches the rhombohedral La_2NiMnO_6 crystal lattice along the $[111]_{cubic}$ direction, triggering a displacement of the *A*-site La ions in the double-perovskite lattice. The lattice distortion and the *A*-site displacements stabilize a ferroelectric polar state in ferromagnetic La_2NiMnO_6 crystals. The ferroelectric state only appears in the rhombohedral La_2NiMnO_6 phase, where MnO_6 and NiO_6 octahedral tilting is inhibited by the threefold crystal symmetry. Electron localization mapping showed that covalent bonding with oxygen and 6*s* orbital lone-pair formation are negligible in this material.

DOI: 10.1103/PhysRevB.91.134107 PACS number(s): 77.80.bn, 77.55.Px, 77.55.Nv

I. INTRODUCTION

The likelihood of a symmetry-breaking ferroelectric atomic displacement occurring at the *B* site of an ABO_3 perovskite can generally be predicted by evaluating the Goldschmidt tolerance factor, $t = (r_O + r_A)/\sqrt{2}(r_O + r_B)$, where r_O, r_A, and r_B are the ionic radii of the oxygen anion and the *A*- and *B*-site cations [1,2]. When $t > 1$, the *B*-site cation in the perovskite lattice has sufficient space to be displaced from the center of a BO_6 octahedron. Conversely, if $t < 1$, an *A*-site displacement would be preferred over a *B*-site shift, as has been predicted theoretically for $K_{0.5}Li_{0.5}NbO_3$ [1] and $LaLuNiMnO_6$ [3]. Experimentally, $Ba_{1-x}Ca_xTiO_3$ ($0.02 < x < 0.34$) single crystals have been shown to exhibit off-center displacements of the smaller Ca ions at the *A* site [4]. However, smaller *A*-site ions generally lead to rotations and tilting of the BO_6 octahedra, which preserves the inversion symmetry by doubling the unit cell [1,2]. For this reason, *A*-site-driven proper ferroelectricity is usually negligible in perovskites.

Well-known exceptions are the Bi- and Pb-containing *A*-site ferroelectric perovskites $Pb(Ti,Zr)O_3$, $BiFeO_3$, and Bi_2NiMnO_6 [5–9]. The Pb and Bi ions in those compounds form covalent bonds with oxygen and contain 6*s* orbital lone pairs, stabilizing a distorted structure and breaking the inversion symmetry. For other *A*-site ions, like Ba and La, it is exceedingly rare to form a covalent bond with oxygen and 6*s* orbital lone pairs in the perovskite lattice. Exceptions can be found in short-period $PbTiO_3/SrTiO_3$ *A*-site ordered superlattices [10] and in *A*-site ordered double perovskites [11,12]. A combination of *A*-site ordering and BO_6 octahedral rotation in epitaxially strained heterostructures has been shown to give rise to improper ferroelectricity.

In this work, we have investigated the possibility of *A*-site-driven ferroelectricity in *B*-site ordered ferromagnetic La_2NiMnO_6 crystals. Based on Kanamori-Goodenough rules [13,14], La_2NiMnO_6 has been theoretically predicted and experimentally reported to show ferromagnetic order due to the presence of 180° Ni^{2+}-O-Mn^{4+} superexchange bonding between an empty Mn^{4+} e_g orbital and a half-filled *d* orbital on a neighboring Ni^{2+} site. The average tolerance factor of La_2NiMnO_6 is 0.97, suggesting the possibility of *A*-site-driven ferroelectricity. However, in bulk crystals, the BO_6 octahedra are tilted and rotated, forming nonpolar rhombohedral ($R\bar{3}$) and monoclinic ($P2_1/n$) structures [15–17].

La_2NiMnO_6 thin films can be grown epitaxially on $LaAlO_3$, $(LaAlO_3)_{0.3}$-$(SrAl_{0.5}Ta_{0.5}O_3)_{0.7}$ (LSAT), and $SrTiO_3$ substrates [18]. Epitaxial strain always shrinks or expands the crystal lattice of a thin film along a certain direction, possibly stabilizing a phase that differs from a strain-free bulk crystal. Even when no strain-related symmetry changes occur in the film, it is common to see Curie temperature shifts in ferroelectrics and ferromagnets [19]. For example, epitaxial strain has been shown to induce ferroelectricity in paraelectric $SrTiO_3$ [20], $SrMnO_3$ [21], and $EuTiO_3$ [22]. In the case of La_2NiMnO_6 films on $LaAlO_3(001)$ substrates, polarized Raman measurements have revealed that the rhombohedral ($R\bar{3}$) and monoclinic ($P2_1/n$) phases coexist at room temperature [23], even though in bulk La_2NiMnO_6 crystals the rhombohedral and monoclinic phases are stabilized at high and low temperatures, respectively [15,16]. Here we theoretically and experimentally investigate the epitaxial strain effect on the dielectric properties of La_2NiMnO_6 thin films and show that epitaxial strain induces ferroelectricity in $La_2NiMnO_6/SrTiO_3$ heterostructures.

II. FIRST-PRINCIPLES DENSITY-FUNCTIONAL CALCULATIONS

The effect of epitaxial strain on the crystal symmetry and polar instability of La_2NiMnO_6 films was studied by density-functional theory (DFT) simulations using the Vienna

*rtaka@issp.u-tokyo.ac.jp

Ab-initio Simulation Package (VASP) within the generalized gradient approximation to the exchange correlation potential [24,25]. The electronic correlation effects were considered by using the generalized gradient approximation (GGA)+U method with $U = 3$ eV for the Mn and Ni d states [26]. It has been reported that La_2NiMnO_6 crystalizes in the rhombohedral structure ($R\bar{3}$) at high temperature and transforms to the monoclinic structure ($P2_1/n$) at low temperature. In fact, these two structures coexist over a wide temperature range [15,16]. The strain effect on the polar instability was studied for both structures. For the rhombohedral structure, the unit cell volume was constrained to the experimentally observed value, $V = 353.33$ Å^3 and converted to a hexagonal structure for the calculation. The c/a ratio was tuned to simulate the strain effect. The cutoff energy for the plane waves was set at 400 eV, whereas the k-point sampling was done using a $4 \times 4 \times 2$ grid in the hexagonal lattice. The Mn and Ni atoms were aligned alternately along the $[111]_{cubic}$ direction with the spins set in a ferromagnetic configuration. The ferroelectric polarization was calculated by using the Berry phase method and comparing the ferroelectric structure and the paraelectric (centrosymmetric) reference structure.

The monoclinic structure did not show spontaneous polarization under any strain field, corroborating the recent work by Zhao *et al.* [12]. In contrast, the rhombohedral La_2NiMnO_6 crystal structure, schematically illustrated in the inset of Fig. 1(a), presented a clear polar state under moderate strain. Figure 1(a) shows the strain dependence of the spontaneous polarization along the $[111]_{cubic}$ direction in a rhombohedral La_2NiMnO_6 crystal. The inset plot shows the relationship between the rhombohedral lattice parameter and the rhombohedral angle. Increasing the tensile strain lowers the rhombohedral angle of the La_2NiMnO_6 crystal and ultimately leads to a polar state when the lattice parameter exceeds 5.7 Å, which corresponds to 4.2% tension with respect to the experimental bulk value of 5.47 Å. A comparison of the partial density of states plots (not shown) of the paraelectric and a 5.9% stretched ($a = 5.79$ Å) ferroelectric phases indicated that the empty La 6s state is very slightly shifted by the structural distortion, whereas the Ni and Mn 3d states remain essentially unaffected.

The crystal structures of the unstrained paraelectric and the +5.9% stretched ferroelectric rhombohedral La_2NiMnO_6 phases are compared in Figs. 1(b) and 1(c). The structural model plots have been oriented along the $[110]_{cubic}$ and $[001]_{cubic}$ directions. The B-site Ni and Mn ions are alternately aligned along the $[111]_{cubic}$ direction. The relaxed structural parameters of the paraelectric and ferroelectric La_2NiMnO_6 phases are listed in Table I. In the paraelectric $R\bar{3}$ structure, the A-site La lattice shows no displacement. By applying a tensile strain field, the crystal symmetry drops from $R\bar{3}$ to $R3$ and the La lattice develops a sizable La displacement along the $[111]_{cubic}$ direction. The mechanism responsible for the La lattice shift fundamentally differs from the Bi lone-pair mechanism seen in ferroelectric $BiFeO_3$ [6–8] and Bi_2NiMnO_6 [9]. The calculated electronic localization function [27] is mapped in Fig. 2 for the $R3$ symmetry of ferroelectric La_2NiMnO_6. No unbalanced charge distributions were found around the La ions, unlike the ferroelectric Bi perovskites that have been reported to exhibit localized lobe-shaped charge distributions surrounding the Bi ions [28]. This indicates that the strain-induced ferroelectricity in rhombohedral La_2NiMnO_6 cannot be attributed to either a 6s orbital lone pair of La or covalent bonding between La and oxygen. The DFT calculation suggests that ferroelectricity and ferromagnetism coexist in the rhombohedral La_2NiMnO_6 lattice when the crystal is stretched along the $[111]_{cubic}$ direction.

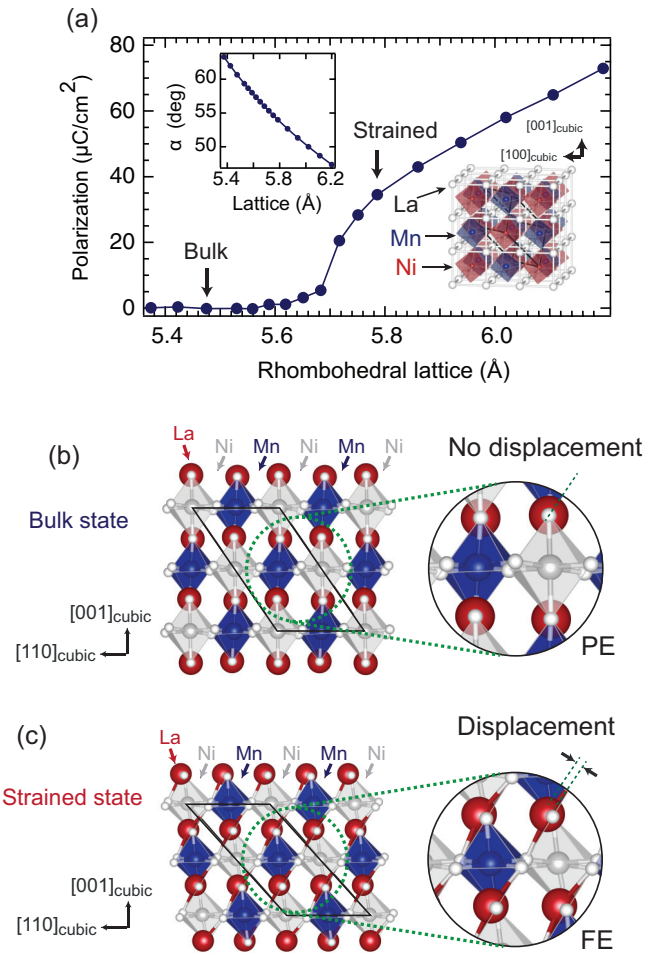

FIG. 1. (Color online) (a) Calculated strain dependence of spontaneous polarization along the $[111]_{cubic}$ direction in a rhombohedral La_2NiMnO_6 lattice. The arrows in the graph mark the experimental bulk (5.47 Å) and strained film lattice constants (5.79 Å). The relationship between the rhombohedral lattice parameter and the rhombohedral angle α is shown in the left inset. The right inset schematically illustrates the rhombohedral La_2NiMnO_6 crystal structure. The B-site Ni (red) and Mn (blue) atoms are alternately aligned along the $[111]_{cubic}$ direction. The black lines mark the rhombohedral unit cell. Schematic illustration of the paraelectric (b) and ferroelectric crystal structure under 5.9% tension (c). The black solid lines denote the rhombohedral La_2NiMnO_6 unit cell. The paraelectric phase exhibits no displacement of the A-site La ions (red). In contrast, a displacement of A-site La ions is clearly visible along the $[111]_{cubic}$ direction in the ferroelectric phase of the strained rhombohedral La_2NiMnO_6 lattice.

TABLE I. Energy-minimized structural parameters of the paraelectric (top) and the ferroelectric (bottom) La_2NiMnO_6 structure under 5.9% tension.

Paraelectric phase: $R\bar{3}$					
a (Å)	α (°)		x	y	z
5.475	60.671	La	0.243	0.243	0.243
		Ni	0	0	0
		Mn	0.500	0.500	0.500
		O	0.787	0.701	0.273
Ferroelectric phase: $R3$, 5.9% tension					
a (Å)	α (°)		x	y	z
5.253	53.997	La	0.272	0.272	0.272
		La	0.773	0.773	0.773
		Ni	0.006	0.006	0.006
		Mn	0.505	0.505	0.505
		O	0.217	0.303	0.749
		O	0.247	0.794	0.704

III. EXPERIMENT

To verify the DFT calculation results experimentally, La_2NiMnO_6 films were grown on $SrTiO_3$ ($c = 3.905$ Å) and LSAT ($c = 3.87$ Å) substrates by pulsed laser deposition (PLD) [29–31]. A polycrystalline stoichiometric La_2NiMnO_6 target, fabricated by conventional solid-state reactions, was ablated with a KrF excimer laser ($\lambda = 248$ nm) at a repetition rate of 5 Hz. During deposition, the $SrTiO_3$ substrates were kept at temperatures between 600 °C and 700 °C and pure oxygen gas was continuously supplied into the growth chamber to maintain an ambient pressure of 500 mTorr. After growth, the films were cooled to 500 °C at a rate of 15 °C/min. The growth chamber was then filled to 760 Torr of pure oxygen gas and the films were cooled down to room temperature.

Basic room-temperature structural analysis was done by x-ray diffraction (XRD) and reciprocal space mapping. As it is difficult to determine the crystal symmetry of La_2NiMnO_6 films by XRD, Raman spectroscopy was used to determine the presence of different crystallographic phases and to look for structure changes below room temperature. A He-Ne laser (633 nm, 17 mW) was focused on the La_2NiMnO_6 film surface through a ×50 objective lens with N.A. = 1.0 for room-temperature measurements and 0.5 for low-temperature measurements. The scattering spectra were collected by a charge-coupled device detector (RAMASCOPE, Renishaw). As the film surface was parallel to the $(001)_{cubic}$ plane, polarized Raman spectra could be taken in exact XX, $X'X'$, XY, and $X'Y'$ scattering configurations, where $X \parallel [110]_{cubic}$, $X' \parallel [100]_{cubic}$, $Y \parallel [\bar{1}10]_{cubic}$, and $Y' \parallel [010]_{cubic}$. The sample temperature was controlled with a He flow cryostat (Microstat, Oxford Instruments).

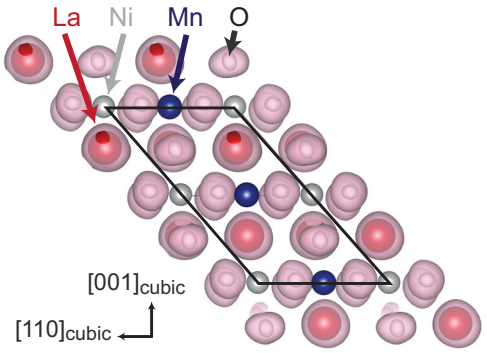

FIG. 2. (Color online) Calculated electron localization functions for the ferroelectric $R3$ structure of La_2NiMnO_6. The La ions are shown in dark red, the Ni ions in gray, the Mn ions in dark blue, the oxygen in white and the electron localization in pink. The black lines mark the rhombohedral unit cell.

The degree of B-site order in La_2NiMnO_6 films can be estimated from the saturation magnetization. The magnetic properties of the films were measured with a superconducting quantum interference device (SQUID) magnetometer.

The presence of ferroelectric order was measured by several complementary techniques to show that the ferroelectricity is indeed an intrinsic feature of the films and not an artifact of temperature- or bias-dependent leak current or interface capacitance changes. For traditional ferroelectric P-E hysteresis measurements, interdigitated Au electrodes were formed on the La_2NiMnO_6 film surfaces by e-beam evaporation and photolithographic lift-off [32]. The Au electrode thickness was 100 nm, the finger width and length were 10 μm and 200 μm, respectively, and the electrode gap was 10 μm. Electrical contacts were made by ultrasonic wire bonding of aluminum wires to the Au pads. The electrical polarization was deduced by integrating the displacement current during a bipolar 15 V triangular bias voltage sweep at 1 Hz.

Positive-up-negative-down (PUND) measurements were performed for detecting the displacement current during ferroelectric domain reversal by an applied bias voltage and eliminate the possibility that the P-E loop measurements might be affected by a bias-dependent interface capacitance change. At first, all ferroelectric domains were poled by a trapezoidal 20 V pulse. Subsequently, two positive and two negative trapezoidal pulses were applied to the La_2NiMnO_6 films. The displacement current was converted to a voltage signal with a current-voltage converter and measured with a digitizer.

Determining the temperature dependence of polarization from P-E measurements can be complicated in thin films by changes in the magnitude of leak currents that may completely mask small displacement currents. A useful technique for measuring the polarization of a thin film sample without having to apply a bias voltage during the measurement is the Chynoweth method of dynamic pyroelectric detection of dielectric polarization. For the pyroelectric measurements [32–35], a 100-nm-thick Pd top electrode was deposited on the La_2NiMnO_6/Nb:$SrTiO_3$ film surface by electron beam evaporation through a stencil mask with 1-mm diameter openings. Chopped light from a semiconductor diode laser (1.63 μm, 100 mW) was focused on a Pd top electrode pad, resulting in a modulation of the La_2NiMnO_6 capacitor temperature and the generation of a pyroelectric current. The sample current was converted to a voltage signal with a current-voltage converter and measured with a lock-in amplifier. The Pd electrode thickness of 100 nm was large enough to eliminate the occurrence of photocurrents under

the 1.63 μm laser illumination. Details of the pyroelectric measurements can be found in Refs. [32–35].

Since polar and nonpolar crystallographic phases are known to coexist in La_2NiMnO_6, a scanning nonlinear dielectric microscope (SNDM) [36,37] was used to image the nanoscale spatial distribution of ferroelectric polar domains at the La_2NiMnO_6 film surface at room temperature. A metal-coated cantilever attached to a 0.8 GHz LC oscillator SNDM probe was used to scan the film surface. A 1 V_{pp}, 23 kHz ac bias was applied between the Nb:$SrTiO_3$ substrate and the probe tip.

IV. RESULTS AND DISCUSSION

A. Structural and magnetic properties of La_2NiMnO_6 films

The degree of spontaneous ordering of B-site ions in double-perovskite thin films can be tuned by varying the film growth temperature and the oxygen pressure, leading to various different magnetic phases, including ferromagnetic, ferrimagnetic, and antiferromagnetic films [29,38]. In this work, ordered and disordered La_2NiMnO_6 films were grown on $SrTiO_3$(001) substrates at 700 °C and 600 °C, respectively. In Fig. 3(a), a reciprocal space map of a $La_2NiMnO_6/SrTiO_3$ sample grown at 700 °C shows a single (206) film reflection in addition to the strong substrate (103) peak. All samples used in this study presented similar coherent growth of La_2NiMnO_6 on both $SrTiO_3$(001) and LSAT(001) substrates. The in-plane and out-of-plane lattice parameters of the strained $La_2NiMnO_6/SrTiO_3$ film were 3.91 Å and 3.85 Å, respectively. In contrast, the lattice parameters of a La_2NiMnO_6/LSAT sample were 3.87 Å and 3.88 Å along the in-plane and out-of-plane directions. The $SrTiO_3$ substrate thus induced tensile strain, stretching the La_2NiMnO_6 lattice along the in-plane direction. The ordering of the B-site Ni and Mn ions was determined from $\theta/2\theta$ XRD measurements performed with a four-circle diffractometer along the $[111]_{cubic}$ direction, as shown in Fig. 3(b). In addition to the $SrTiO_3$ (lll) substrate peaks, all La_2NiMnO_6 (lll) reflections can be clearly seen. Small peaks of odd-l La_2NiMnO_6 (lll) reflections correspond to the ordered B-site superlattice of Ni and Mn ions along the $[111]_{cubic}$ direction. The inset shows details of the La_2NiMnO_6(333) reflection. The dashed line marks the expected peak position of a nonstrained bulk La_2NiMnO_6 crystal, showing that the B-site ordered La_2NiMnO_6 film on the $SrTiO_3$ substrate was stretched by +1.1% along the $[111]_{cubic}$ direction by the epitaxial strain.

Rhombohedral and monoclinic phases have been reported to coexist in La_2NiMnO_6 at room temperature [23]. Even in a phase-pure rhombohedral La_2NiMnO_6 film grown on a $SrTiO_3$(001) substrate, four reflection peaks should be visible in a reciprocal space map around the $SrTiO_3$(103) reflection. The overlapping diffraction peaks of multiple domains of two possible phases make detailed structural analysis difficult with a laboratory x-ray source. Due to this, the reciprocal space map in Fig. 3(a) shows only a single peak originating from the La_2NiMnO_6 film. In order to accurately analyze the La_2NiMnO_6 film structure, polarized Raman measurements were performed on the ordered $La_2NiMnO_6/SrTiO_3$ films at room temperature, as shown in Fig. 4(a). The main benefit of

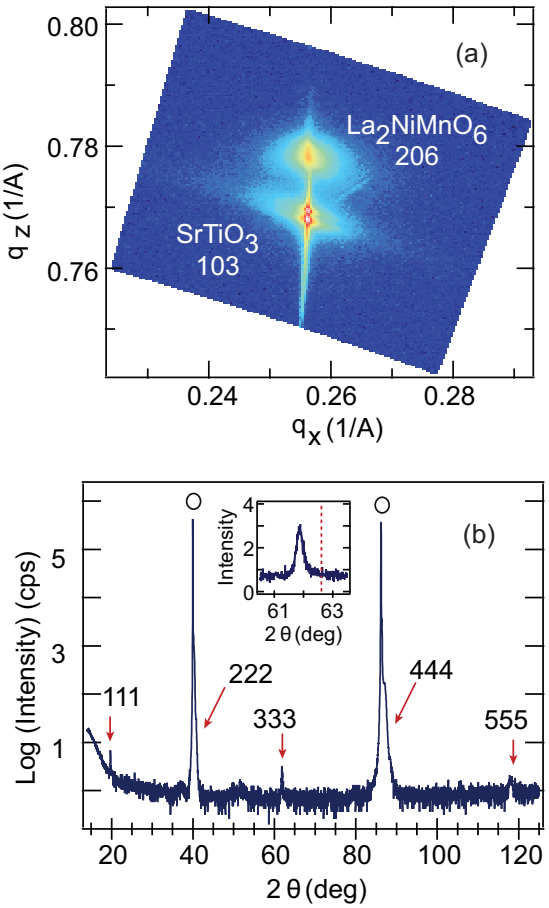

FIG. 3. (Color online) (a) XRD reciprocal space map around the $SrTiO_3$ substrate $(103)_{cubic}$ reflection of a $La_2NiMnO_6/SrTiO_3$ film, confirming coherent growth of the La_2NiMnO_6 film on the substrate. (b) XRD pattern of the La_2NiMnO_6 film along the $SrTiO_3$ substrate $[111]_{cubic}$ direction, indicating that the B-site Ni and Mn ions are ordered. Details of the $(333)_{cubic}$ reflection are shown in the inset. The dashed line marks the expected bulk peak position, indicating that the La_2NiMnO_6 film crystal is stretched by +1.1% along the $[111]_{cubic}$ direction by epitaxial strain.

the Raman measurement is the ability to distinguish between the rhombohedral and monoclinic phases in the film.

Except for small differences in phonon line parameters, the spectra and their variation with scattering configuration closely resemble those reported for $La_2NiMnO_6/LaAlO_3$(001) films [23], indicating that rhombohedral and monoclinic phases coexist in our $La_2NiMnO_6/SrTiO_3$ films as well. In particular, the presence of three peaks in a $X'Y'$ spectrum can be used to detect the presence of the rhombohedral phase, because the monoclinic phase should not exhibit any $X'Y'$ scattering peaks.

In order to investigate the stability of the rhombohedral and monoclinic phases at low temperature, the temperature dependence of XX and XY Raman spectra was investigated from 5 K to 300 K, as shown in Figs. 4(b) and 4(c). The spectra show that both rhombohedral and monoclinic phases coexist over the whole temperature range.

In general, the Raman peak position (ω_{anh}) has a temperature dependence of $\omega_{anh}(T) = \omega_0 - C(1 + \frac{2}{e^{\hbar\omega_0/kT}-1})$, with

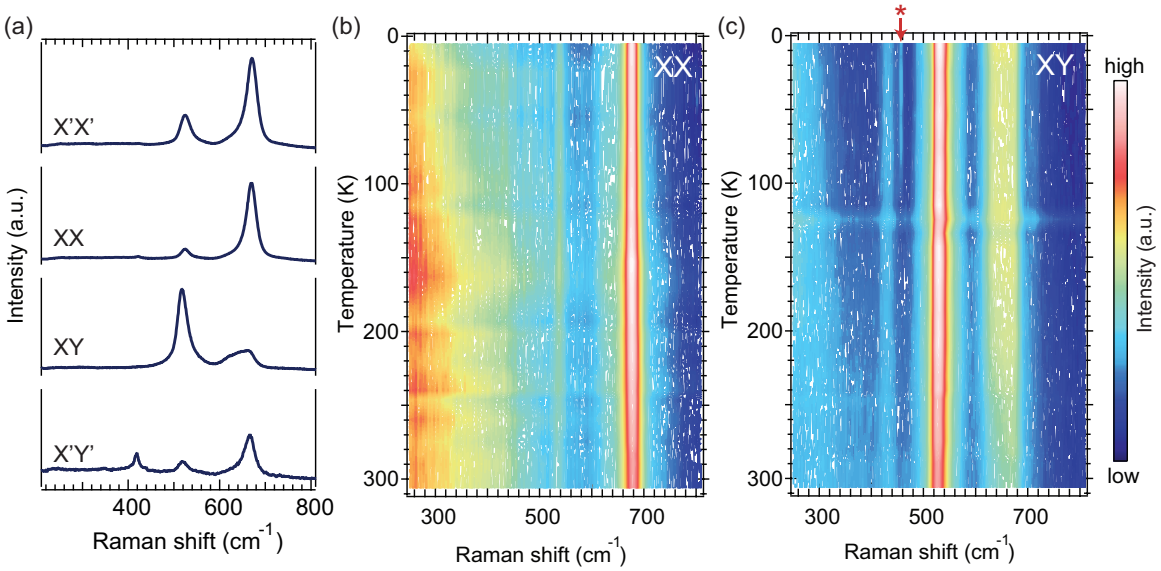

FIG. 4. (Color online) (a) Polarized Raman spectra of an ordered $La_2NiMnO_6/SrTiO_3$ film obtained at room temperature, showing that rhombohedral and monoclinic phases coexist. Temperature dependence of XX (b) and XY (c) Raman spectra of a B-site ordered $La_2NiMnO_6/SrTiO_3$ film between 5 K and 300 K. The red arrow in (c) marks the 457 cm^{-1} peak that appears below 105 K.

ω_0 and C being adjustable parameters. The Raman peak positions should thus shift to higher wave numbers as the temperature is decreased. In Figs. 4(b) and 4(c), only the peak at 660–700 cm^{-1} in the XX spectra shows a detectable temperature dependence, shifting from 678.51 cm^{-1} at 300 K to 676.73 cm^{-1} at 5 K, indicating anomalous phonon softening. Similar softening caused by spin-phonon coupling has been observed in other double-perovskite systems, such as $La_2NiMnO_6/LaAlO_3$ [23] and $La_2CoMnO_6/SrTiO_3$ [39]. Spin-phonon coupling can stabilize a ferroelectric state in epitaxially strained ferromagnetic crystals, as happens in ferroelectric and ferromagnetic $EuTiO_3$ thin films grown on $DyScO_3$ substrates [19,22]. A similar mechanism may be expected to trigger ferroelectricity in strained ferromagnetic La_2NiMnO_6 films.

Besides peak shifts, a small peak, marked by an arrow in Fig. 4(c), appeared at 457 cm^{-1} in the XY spectra below 105 K. A similar low-temperature behavior was observed for a disordered $La_2NiMnO_6/SrTiO_3$ film. The $SrTiO_3$ substrate crystal undergoes an antiferrodistortive structural transition from a high-temperature cubic phase to a low-temperature tetragonal phase at 105 K, resulting in a 0.015% in-plane lattice parameter change [40]. The epitaxial strain imposed on the film by the $SrTiO_3$ substrate thus changes slightly at this temperature, resulting in a discontinuous temperature dependence of the Raman spectra in La_2NiMnO_6 samples. The reduction of the crystal symmetry of a La_2NiMnO_6 film can therefore be expected to enhance the ferroelectric polarization at temperatures below 105 K.

The level of B-site order can be quantified by looking at the magnetization of the films, as shown in Fig. 5(a). The magnetization hysteresis loops were measured at 10 K for ordered and disordered $La_2NiMnO_6/SrTiO_3$ samples. By comparing the observed saturation magnetizations of the films with the theoretical magnetization of 2.5 μ_B/B-site for a perfectly ordered La_2NiMnO_6 crystal [13,14], the fraction of B-site order in the ordered and disordered La_2NiMnO_6 films can be estimated to be 80% and 26%, respectively. Figure 5(b) presents the temperature dependence of the field-cooled and zero-field-cooled magnetizations at 0.75 T for the

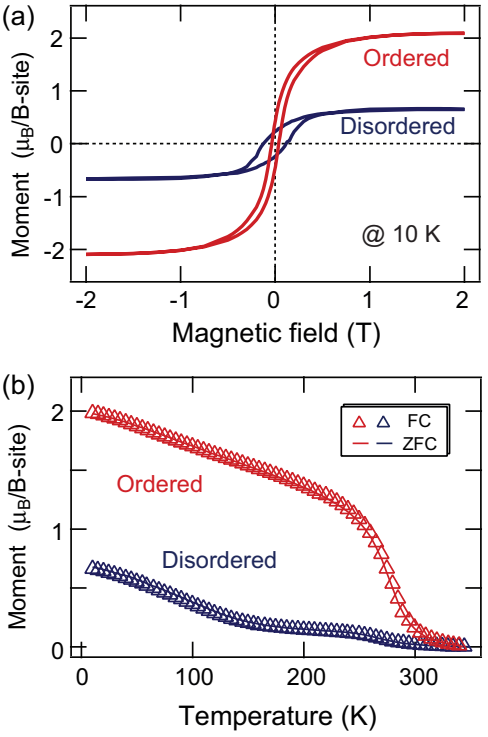

FIG. 5. (Color online) (a) Magnetization hysteresis loops at 10 K for ordered and disordered La_2NiMnO_6 films on $SrTiO_3$ substrates. (b) Temperature dependence of the magnetic moment at 0.75 T, showing that the magnetic Curie temperature is close to 280 K, corresponding to the reported bulk value.

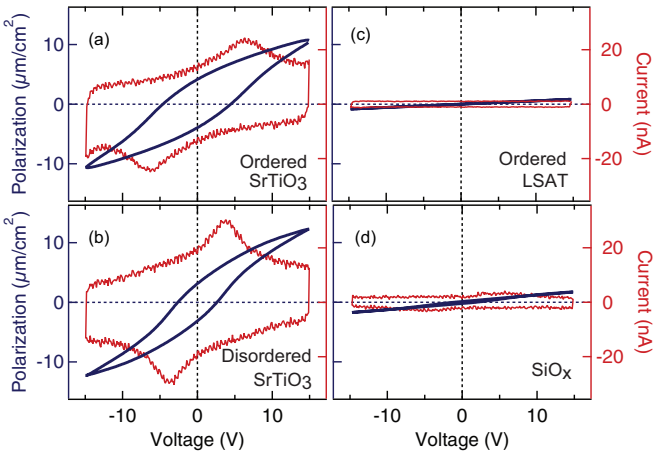

FIG. 6. (Color online) Ferroelectric polarization (left axis) and displacement current (right axis) as a function of applied voltage at 10 K for ordered (a) and disordered (b) $La_2NiMnO_6/SrTiO_3$ films, an ordered La_2NiMnO_6/LSAT film (c), and a nonferroelectric $SiO_x/SrTiO_3$ (d) reference sample.

same samples. The magnetic Curie temperature is 280 K in both cases, matching reported values [15]. The magnetization data suggests that the ordered (80%) and disordered (26%) $La_2NiMnO_6/SrTiO_3$ samples were ferromagnetic and ferrimagnetic, respectively.

B. Ferroelectric properties of La_2NiMnO_6 films

The presence of spontaneous polarization was determined in ordered and disordered $La_2NiMnO_6/SrTiO_3$ films, as well as an ordered La_2NiMnO_6/LSAT sample by measuring the ferroelectric polarization and the displacement current in the in-plane direction at 10 K as shown in Fig. 6. Both films grown on $SrTiO_3$ substrates were verified to exhibit ferroelectric domain reversal under an external electric field, while the La_2NiMnO_6/LSAT sample showed no hysteresis behavior at all, revealing the importance of strain in the formation of a ferroelectric state in the $La_2NiMnO_6/SrTiO_3$ films. There is little difference in ferroelectric polarization between the ordered and disordered $La_2NiMnO_6/SrTiO_3$ films. This is consistent with the calculation results in Fig. 1, which showed that the *B*-site Ni and Mn ions do not have a significant effect on the *A*-site-driven ferroelectricity in La_2NiMnO_6 films. Moreover, this data can rule out improper ferroelectricity originating from bond- and site-centered charge ordering, as happens in Fe_3O_4 crystals [32,34,41] and the *E*-type antiferromagnetic order that can be found in Y_2CoMnO_6 and Lu_2CoMnO_6 crystals [41–43].

We note that when measuring the ferroelectric polarization in thin films grown on $SrTiO_3$ substrates, it is important to verify that the substrate material does not contribute to the observed signal [32]. It has been reported that an electric field of 700 V/mm can induce a polarization of $\approx 1\ \mu C/cm^2$ in $SrTiO_3$ crystals [44]. To rule out the effect of the substrate on the La_2NiMnO_6 film measurements, a nonferroelectric SiO_x film with a thickness of 100 nm was grown on a $SrTiO_3$(001) substrate by thermal evaporation. After annealing the film at 400 °C in air and depositing identical interdigitated

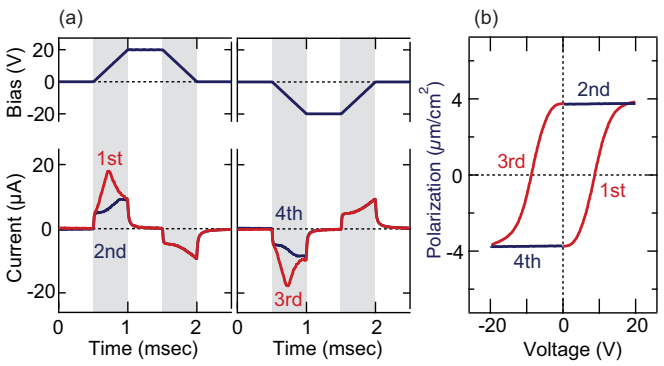

FIG. 7. (Color online) (a) PUND measurements at 10 K for an ordered $La_2NiMnO_6/SrTiO_3$ sample. Only the first and third pulses showed a displacement current due to the reversal of ferroelectric domains. (b) Ferroelectric polarization hysteresis loop calculated from the PUND measurements in (a).

Au electrodes, ferroelectric hysteresis measurements were performed at 10 K. Figure 6(d) shows the hysteresis loop and displacement current of a $SiO_x/SrTiO_3$ film for comparison with the ordered and disordered $La_2NiMnO_6/SrTiO_3$ films. The $SiO_x/SrTiO_3$ sample did not show a hysteresis loop, proving that the hysteresis loops obtained for the ordered and disordered $La_2NiMnO_6/SrTiO_3$ films originated from ferroelectricity in the films.

Successful observation of ferroelectric hysteresis loops means that leakage currents in the La_2NiMnO_6 films were low compared to the displacement current that arises when the ferroelectric polarization is reversed by an applied bias. However, this type of direct hysteresis measurements is generally not a reliable method for measuring the spontaneous polarization in ferroelectric oxide thin films because the measured current consists of several components due to switching of the ferroelectric domains, the linear dielectric response, and leakage current of the material. Particularly for La_2NiMnO_6 films, the intermixed nonferroelectric monoclinic phase would produce a linear dielectric response when an electric field is applied, resulting in an increase of the background current. To suppress the linear dielectric behavior during hysteresis measurements, PUND measurements were performed for the ordered $La_2NiMnO_6/SrTiO_3$ sample, as shown in Fig. 7(a).

Only the first and third pulses showed domain reversal displacement currents, proving that the $La_2NiMnO_6/SrTiO_3$ film was indeed ferroelectric. The advantage of PUND measurements is to eliminate the linear dielectric current contribution by subtracting the second (fourth) cycle current from the first (third) cycle one. Figure 7(b) presents the ferroelectric hysteresis loop measured in this way, exhibiting a fully saturated loop with a spontaneous polarization of $3.8\ \mu C/cm^2$. The PUND measurement shows that the spontaneous polarization of the La_2NiMnO_6 layer is slightly lower than the remanent polarization seen in the standard hysteresis measurements in Fig. 6(a), which include a linear dielectric response component.

The temperature dependence of ferroelectric hysteresis loop shapes is presented in Fig. 8(a), together with the temperature dependence of the remanent polarization in Fig. 8(b). The remanent ferroelectric polarizations of ordered and disordered

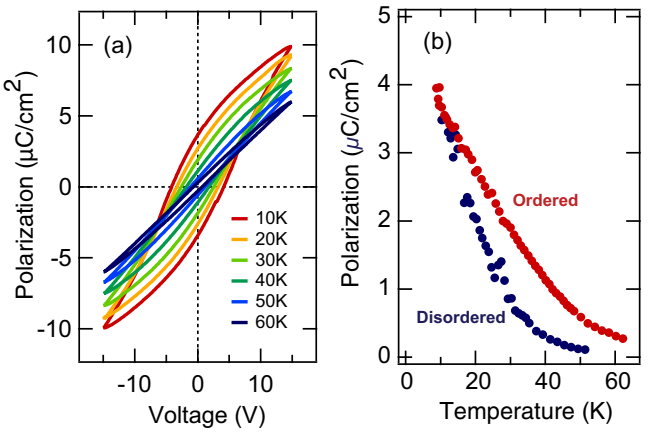

FIG. 8. (Color online) (a) Comparison of P-E hysteresis loop shapes measured from 10 K to 60 K. (b) Temperature dependence of the remanent polarization of ordered and disordered La_2NiMnO_6 films.

$La_2NiMnO_6/SrTiO_3$ films were estimated to be 4.2 $\mu C/cm^2$ and 3.2 $\mu C/cm^2$, respectively, from the hysteresis loops measured at 10 K, and gradually decreased to zero at around 50 to 60 K as the temperature was increased.

To precisely evaluate the polar state in $La_2NiMnO_6/SrTiO_3$ films, dynamic pyroelectric measurements [32–34] were performed for the ordered and disordered La_2NiMnO_6/Nb:$SrTiO_3$(001) samples, as shown in Fig. 9. In this case, the temperature derivative of the spontaneous polarization was measured along the out-of-plane direction. Below 250 K, the pyroelectric response increased for both samples with decreasing temperature. The maximum pyroelectric signal amplitude was observed at 100 to 150 K, below which the pyroelectric response decreased. A clear kink can be seen in the pyroelectric current amplitude at 105 K, as marked by arrows in Fig. 9. This is related to the abrupt change observed in the Raman measurements in Fig. 4(c). The 105 K structural transition in the $SrTiO_3$ substrate crystal

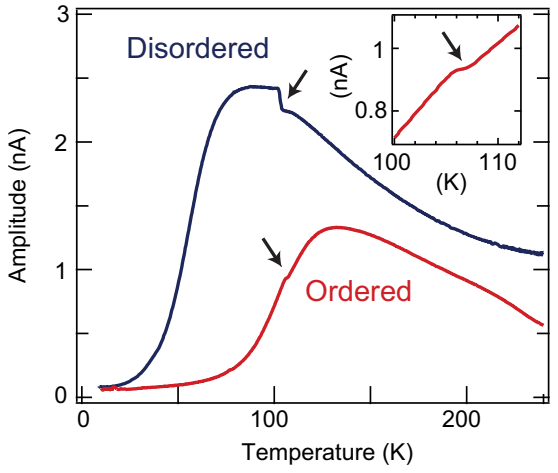

FIG. 9. (Color online) Temperature dependence of the pyroelectric response for ordered (red) and disordered (blue) $La_2NiMnO_6/SrTiO_3$. The inset shows the pyroelectric response of the ordered film sample close to 105 K.

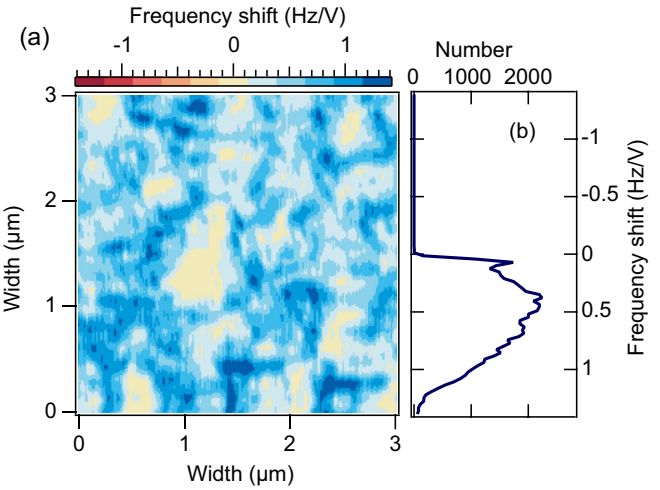

FIG. 10. (Color online) (a) SNDM image of an ordered $La_2NiMnO_6/SrTiO_3$ film surface at room temperature. (b) The histogram of the SNDM signal reveals that most ferroelectric domains are negatively polarized. Regions where the frequency shift is zero correspond to the intermixed monoclinic phase.

causes a stepwise 0.015% change in the epitaxial strain on the La_2NiMnO_6 film lattice, resulting in a discontinuous temperature dependence of the pyroelectric responses in both samples. This result is a clear indication that ferroelectricity in $La_2NiMnO_6/SrTiO_3$ films is very sensitive to epitaxial strain.

The ferroelectric domain structure of the films was determined by acquiring SNDM [36,37] images at room temperature. Figure 10(a) shows a typical SNDM image for an ordered La_2NiMnO_6/Nb:$SrTiO_3$ film. The observation of a uniform SNDM frequency shift signal indicates that the $La_2NiMnO_6/SrTiO_3$ film was spontaneously polarized at room temperature. The histogram in Fig. 10(b) shows that most areas were polarized with a negative charge at the top surface, matching the polarization direction determined by the pyroelectric analysis. Some regions exhibited a zero frequency shift, indicating that there was no vertical spontaneous polarization in these parts of the La_2NiMnO_6/Nb:$SrTiO_3$ film, probably due to the intermixing of the nonpolar monoclinic phase that was detected in the Raman measurements.

According to the DFT calculations, a ferroelectric distortion appears only in the rhombohedral La_2NiMnO_6 phase when the crystal is stretched along the $[111]_{cubic}$ direction. The monoclinic structure lacks the threefold rotation, allowing antiphase tilting of the MnO_6 and NiO_6 octahedra, which suppresses the La polar distortion and results in a paraelectric state. In contrast, the rhombohedral structure preserves the threefold rotation symmetry that does not allow MnO_6 and NiO_6 octahedral tilting but allows polar ionic shifts of La. Therefore, ferroelectricity is induced only in a strained $La_2NiMnO_6/SrTiO_3$ film and cannot appear in bulk La_2NiMnO_6.

V. CONCLUSION

We have theoretically and experimentally demonstrated the presence of strain-induced ferroelectricity in ferromagnetic

La_2NiMnO_6 films. Theoretical calculations and tolerance factor analysis indicated the presence of *A*-site-driven ferroelectricity along the $[111]_{cubic}$ direction in epitaxially strained La_2NiMnO_6 crystals. A polar state was shown to exist in epitaxial La_2NiMnO_6 films even at room temperature. The observation of *A*-site ferroelectricity in epitaxially strained La_2NiMnO_6 films highlights the potential of strain engineering for tailoring the properties of complex oxides and extending their functionalities for new device applications.

ACKNOWLEDGMENTS

This study was partly supported by JSPS KAKENHI (Grants No. 26105002, No. 25706022, No. 24740235, and No. 23226008). This work was also partly supported by the Kurata Memorial Hitachi Science and Technology Foundation and the Iketani Science and Technology Foundation. M.K. acknowledges financial support from the Japan Society for the Promotion of Science for young scientists. The authors thank N. Chinone for technical support in using the SNDM.

[1] D. I. Bilc and D. J. Singh, Frustration of tilts and A-site Driven ferroelectricity in $KNbO_3$-$LiNbO_3$ alloys, Phys. Rev. Lett. **96**, 147602 (2006).

[2] N. A. Benedek and C. J. Fennie, Why are there so few perovskite ferroelectrics? J. Phys. Chem. C **117**, 13339 (2013).

[3] D. J. Singh and C. H. Park, Polar behavior in a magnetic perovskite from A-site size disorder: A density functional study, Phys. Rev. Lett. **100**, 087601 (2008).

[4] D. Fu, M. Itoh, S.Y. Koshihara, T. Kosugi, and S. Tsuneyuki, Anomalous phase diagram of ferroelectric (Ba,Ca)TiO_3 single crystals with giant electromechanical response, Phys. Rev. Lett. **100**, 227601 (2008).

[5] R. E. Cohen, Origin of ferroelectricity in perovskite oxides, Nature **358**, 136 (1992).

[6] J. Wang, J. B. Neaton, H. Zheng, V. Nagarajan, S. B. Ogale, B. Liu, D. Viehland, V. Vaithyanathan, D. G. Schlom, U. V. Waghmare, N. A. Spaldin, K. M. Rabe, M. Wuttig, and R. Ramesh, Epitaxial $BiFeO_3$ multiferroic thin film heterostructures, Science **299**, 1719 (2003).

[7] N. A. Hill, Why are there so few magnetic ferroelectrics? J. Phys. Chem. B **104**, 6694 (2000).

[8] J. B. Neaton, C. Ederer, U. V. Waghmare, N. A. Spaldin, and K. M. Rabe, First-principles study of spontaneous polarization in multiferroic $BiFeO_3$, Phys. Rev. B **71**, 014113 (2005).

[9] M. Azuma, K. Takata, T. Saito, S. Ishiwata, Y. Shimakawa, and M. Takano, Designed ferromagnetic, ferroelectric Bi_2NiMnO_6, J. Am. Chem. Soc. **127**, 8889 (2005).

[10] E. Bousquet, M. Dawber, N. Stuck, C. Lichtensteiger, P. Hermet, S. Gariglio, J. M. Triscone, and P. Ghosez, Improper ferroelectricity in perovskite oxide artificial superlattices, Nature **452**, 732 (2008).

[11] J. M. Rondinelli and C. J. Fennie, Octahedral rotation-induced ferroelectricity in cation ordered perovskites, Adv. Mater. **24**, 1961 (2012).

[12] H. J. Zhao, W. Ren, Y. Yang, J. Iniguez, X. M. Chen, and L. Bellaiche, Near room-temperature multiferroic materials with tunable ferromagnetic and electrical properties, Nat. Commun. **5**, 4021 (2014).

[13] J. B. Goodenough, Theory of the role of covalence in the perovskite-type manganites [La,*M*(II)]MnO_3, Phys. Rev. **100**, 564 (1955).

[14] J. Kanamori, Superexchange interaction and symmetry properties of electron orbitals, J. Phys. Chem. Solids **10**, 87 (1959).

[15] N. S. Rogado, J. Li, A. W. Sleight, and M. A. Subramanian, Magnetocapacitance and magnetoresistance near room temperature in a ferromagnetic semiconductor: La_2NiMnO_6, Adv. Mater. **17**, 2225 (2005).

[16] C. L. Bull, D. Gleeson, and K. S. Knight, Determination of B-site ordering and structural transformations in the mixed transition metal perovskites La_2CoMnO_6 and La_2NiMnO_6, J. Phys. Condens. Matter. **15**, 4927 (2003).

[17] H. Das, U. V. Waghmare, T. Saha-Dasgupta, and D. D. Sarma, Electronic structure, phonons, and dielectric anomaly in ferromagnetic insulating double perovskite La_2NiMnO_6, Phys. Rev. Lett. **100**, 186402 (2008).

[18] M. Hashisaka, D. Kan, A. Masuno, M. Takano, Y. Shimakawa, T. Terashima, and K. Mibu, Epitaxial growth of ferromagnetic La_2NiMnO_6 with ordered double-perovskite structure, Appl. Phys. Lett. **89**, 032504 (2006).

[19] D. G. Schlom, L. Q. Chen, C. J. Fennie, V. Gopalan, D. A. Muller, X. Pan, R. Ramesh, and R. Uecker, Elastic strain engineering of ferroic oxides, MRS Bull. **39**, 118 (2014).

[20] N. A. Pertsev, A. K. Tagantsev, and N. Setter, Phase transitions and strain-induced ferroelectricity in $SrTiO_3$ epitaxial thin films, Phys. Rev. B **61**, R825 (2000).

[21] J. H. Lee and K. M. Rabe, Epitaxial-Strain-Induced multiferroicity in $SrMnO_3$ from first principles, Phys. Rev. Lett. **104**, 207204 (2010).

[22] J. H. Lee, L. Fang, E. Vlahos, X. Ke, Y. W. Jung, L. F. Kourkoutis, J. W. Kim, P. J. Ryan, T. Heeg, M. Roeckerath, V. Goian, M. Bernhagen, R. Uecker, P. C. Hammel, K. M. Rabe, S. Kamba, J. Schubert, J. W. Freeland, D. A. Muller, C. J. Fennie, P. Schiffer, V. Gopalan, E. Johnston-Halperin, and D. G. Schlom, A strong ferroelectric ferromagnet created by means of spin-lattice coupling, Nature **466**, 954 (2010).

[23] M. N. Iliev, H. Guo, and A. Gupta, Raman spectroscopy evidence of strong spin-phonon coupling in epitaxial thin films of the double perovskite La_2NiMnO_6, Appl. Phys. Lett. **90**, 151914 (2007).

[24] G. Kresse and J. Furthmuller, Efficient iterative schemes for *ab initio* total-energy calculations using a plane-wave basis set, Phys. Rev. B **54**, 11169 (1996).

[25] J. P. Perdew, K. Burke, and M. Ernzerhof, Generalized gradient approximation made simple, Phys. Rev. Lett. **77**, 3865 (1996).

[26] Y. M. Zhu, D. Ke, R. Yu, Y. H. Hsieh, H. J. Liu, P. P. Liu, Y. H. Chu, and Q. Zhan, Electronic and magnetic properties of La_2NiMnO_6 and La_2CoMnO_6 with cationic ordering, Appl. Phys. Lett. **100**, 062406 (2012).

[27] B. Silvi and A. Savin, Classification of chemical bonds based on topological analysis of electron localization functions, Nature **371**, 683 (1994).

[28] P. Baettig, C. F. Schelle, R. LeSar, U. V. Waghmare, and N. A. Spaldin, Theoretical prediction of new high-performance lead-free piezoelectrics, Chem. Mater. **17**, 1376 (2005).

[29] M. Kitamura, I. Ohkubo, M. Kubota, Y. Matsumoto, H. Koinuma, and M. Oshima, Ferromagnetic properties of epitaxial La_2NiMnO_6 thin films grown by pulsed laser deposition, Appl. Phys. Lett. **94**, 132506 (2009).

[30] M. Kitamura, I. Ohkubo, M. Matsunami, K. Horiba, H. Kumigashira, Y. Matsumoto, H. Koinuma, and M. Oshima, Electronic structure characterization of La_2NiMnO_6 epitaxial thin films using synchrotron-radiation photoelectron spectroscopy and optical spectroscopy, Appl. Phys. Lett. **94**, 262503 (2009).

[31] Y. Sakurai, I. Ohkubo, Y. Matsumoto, H. Koinuma, and M. Oshima, Influence of substrates on epitaxial growth of B-site-ordered perovskite La_2NiMnO_6 thin films, J. Appl. Phys. **110**, 063913 (2011).

[32] R. Takahashi, Y. Cho, and M. Lippmaa, Interfacial capacitance between a ferroelectric Fe_3O_4 thin film and a semiconducting Nb:$SrTiO_3$ substrate, J. Appl. Phys. **117**, 014104 (2015).

[33] R. Takahashi, T. Tybell, and M. Lippmaa, Sub-bandgap photocurrent effects on dynamic pyroelectric measurements in Pt/$PbTiO_3$/Nb:$SrTiO_3$ heterostructures, J. Appl. Phys. **112**, 014111 (2012).

[34] R. Takahashi, H. Misumi, and M. Lippmaa, Pyroelectric detection of spontaneous polarization in magnetite thin films, Phys. Rev. B **86**, 144105 (2012).

[35] R. Takahashi, M. Katayama, O. Dahl, J. K. Grepstad, Y. Matsumoto, and T. Tybell, Epilayer control of photodeposited materials during UV photocatalysis, Appl. Phys. Lett. **94**, 232901 (2009).

[36] Y. Cho, A. Kirihara, and T. Saeki, Scanning nonlinear dielectric microscope, Rev. Sci. Instrum. **67**, 2297 (1996).

[37] Y. Cho, Scanning nonlinear dielectric microscopy, J. Mater. Res. **26**, 2007 (2011).

[38] A. Ohtomo, S. Chakraverty, H. Mashiko, T. Oshima, and M. Kawasaki, Spontaneous atomic ordering and magnetism in epitaxially stabilized double perovskites, J. Mater. Res. **28**, 689 (2013).

[39] M. N. Iliev, M. V. Abrashev, A. P. Litvinchuk, V. G. Hadjiev, H. Guo, and A. Gupta, Raman spectroscopy of ordered double perovskite La_2CoMnO_6 thin films, Phys. Rev. B **75**, 104118 (2007).

[40] A. Okazaki and M. Kawaminami, Lattice constant of strontium titanate at low temperatures, Mater. Res. Bull. **8**, 545 (1973).

[41] J. Brink and D. I. Khomskii, Multiferroicity due to charge ordering, J. Phys.: Condens. Mater. **20**, 434217 (2008).

[42] G. Sharma, J. Saha, S. D. Kaushik, V. Siruguri, and S. Patnaik, Magnetism driven ferroelectricity above liquid nitrogen temperature in Y_2CoMnO_6, Appl. Phys. Lett. **103**, 012903 (2013).

[43] S. Yanez-Vilar, E. D. Mun, V. S. Zapf, B. G. Ueland, J. S. Gardner, J. D. Thompson, J. Singleton, M. Sánchez-Andújar, J. Mira, N. Biskup, M. A. Senaris-Rodriguez, and C. D. Batista, Multiferroic behavior in the double-perovskite Lu_2CoMnO_6, Phys. Rev. B **84**, 134427 (2011).

[44] J. Hemberger, P. Lunkenheimer, R. Viana, R. Bohmer, and A. Loidl, Electric-field-dependent dielectric constant and nonlinear susceptibility in $SrTiO_3$, Phys. Rev. B **52**, 13159 (1995).